THE ASTRONOMICAL JOURNAL, 116:981–986, 1998 August

RADII AND EFFECTIVE TEMPERATURES FOR K AND M GIANTS AND SUPERGIANTS. II.

H. M. DYCK
Department of Astrometry, US Naval Observatory, Navy Prototype Optical Interferometer, Rural Route 14, Box 447, Flagstaff, AZ 86001; meldyck@sextans.lowell.edu

G. T. VAN BELLE[1]
Jet Propulsion Laboratory, Mail Stop 306-388, 4800 Oak Grove Drive, Pasadena, CA 91109; gerard@huey.jpl.nasa.gov

AND

R. R. THOMPSON[1]
Department of Physics and Astronomy, University of Wyoming, Laramie, WY 82071; thompson@sparky.uwyo.edu
Received 1998 February 10; revised 1998 April 7

ABSTRACT

We present new interferometric observations for 74 luminous red stars, made in the near-infrared. We show that our 2.2 μm uniform-disk diameters agree with other near-infrared diameter determinations (lunar occultations and interferometers) for 22 stars measured in common with ours. From our new data, we derive effective temperatures that are compared with our previous work and with comparable observations made by lunar occultations at Kitt Peak. The combined data set yields 91 luminosity class II, II–III, and III stars that have well-determined spectral types spanning the range from about K0 to about M8. There are 83 stars in the sample that define an approximately linear relationship between spectral type and effective temperature for giants, with a dispersion of 192 K at each spectral type. Eight of the stars have temperatures that are roughly 750 K too low for their spectral types. These stars are not known to be at the high-luminosity end of the range of stars observed and are not recognized as binary stars. At present, we have no explanation for their low effective temperatures. We also show that *Hipparcos* parallaxes, combined with our angular diameters, yield linear radii precise enough to see differences in the average radius between luminosity class II and luminosity class III stars.

Key words: stars: fundamental parameters — stars: late-type

1. INTRODUCTION

Measurements of the angular diameters for oxygen-rich giants and supergiants at 2.2 μm have been a long-term goal at the Infrared Optical Telescope Array (IOTA) since first fringes were obtained in late 1993. In this paper, we report new visibility observations for 74 evolved stars. We felt that it was timely to publish the data so that they would nearly coincide with the release of the parallax data set from *Hipparcos*. The combination of well-determined angular diameters with distances will lead to a large body of linear diameters for the upper right part of the H-R diagram. Although we have a larger body of observations than we report here, we restrict the present discussion to stars with observed average visibility levels $V \leq 0.8$. These stars are well enough resolved that the resulting errors in the effective temperature are $\sigma_T \leq 300$ K.

A complete description of the interferometer may be found in Carleton et al. (1994); the methods used to observe fringes and reduce the fringe data to uniform-disk (UD) angular diameters have been described by Dyck et al. (1996, hereafter Paper I). In Paper I, we discussed the advantages of observing at 2.2 μm, compared with both shorter and longer wavelengths. We will not repeat these discussions here, although we stress that we are generally using the fringe visibility at a single spatial frequency point to determine the UD diameter.

This method appears to be sufficiently accurate for giants and supergiants, but it may lead to errors for Mira variables (see, e.g., Tuthill 1994); there are no known Mira variables in the present sample of stars. As an example of the accuracy of this method for characterizing the angular diameter of a star, we show our accumulated data for the M5 supergiant α^1 Her taken at IOTA and the Infrared Michaelson Array (IRMA; see Dyck, Benson, & Ridgway 1993) in Figure 1. A simple UD visibility function, with $\theta_{UD} = 33.2 \pm 0.8$ mas, has been fitted to the data. One may see that there is no systematic departure from the UD function at spatial frequencies lower than the first zero. Beyond the first zero the observed data also fit the UD well, although there may be a small amount of excess power (1%–2%) that could originate in surface structure, such as spots or limb brightening. The quality of the data is not sufficiently high to be able to judge that point at the present time. Because the UD fits this extended atmosphere supergiant well, we expect that the results for less extended luminosity class III stars will be at least as good. Thus, we feel justified in determining the angular diameter for luminosity I, II, and III stars from a single observation of the visibility made at one spatial frequency point. Note also that the comparison of the IRMA and IOTA data, taken at epochs differing by about 4 yr, sets a limit on the amount of variability over this timescale.

We have also compared our angular diameter measurements with those taken by other observing methods, including lunar occultations at 1.65 and 2.2 μm and interferometry at 2.2 μm at CERGA and at IOTA with the FLUOR beam combination system. The references to these other diameter measurements are White & Feierman (1987) for the occultations, Di Benedetto & Rabbia (1987) and Di Benedetto & Ferluga (1990) for the CERGA observations, and Perrin et al. (1998) for the FLUOR data. The comparisons are shown in Figure 2 for the 22 stars measured in common, and the agreement can be seen to be good. If we fit

[1] NASA Space Grant Fellow.

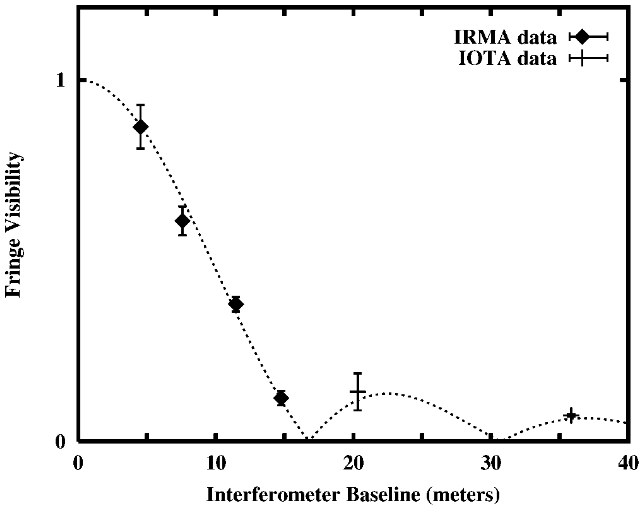

FIG. 1.—Plot of 2.2 μm visibility data for the M5 supergiant α^1 Her with a UD visibility function plotted for comparison. Note that there is no apparent systematic difference between the observations and the simple model for this atmospherically extended star. This is used as justification for deriving the angular diameter for giants and supergiants from a single observation of the visibility at one spatial frequency point.

a line to the data, then the IOTA observations differ in slope by 3.8% from the other observations and have an offset at the origin of about -0.6 mas. Note that, compared with IOTA, the lunar occultation technique is a completely different method for obtaining angular diameters, CERGA is a different interferometer with a different method of estimating fringe visibility, and FLUOR is the same interferometer but with a different beam combination scheme.

2. OBSERVATIONS

The new data are reported in Table 1, where we have given the Bright Star Catalogue (Hoffleit 1982) number, a common name or other identifier, the date of the observation, the projected interferometer baseline, the visibility and the UD angular diameter, and an associated error. Because the interferometer response is not constant, as a result of mechanical changes in the instrument and atmospheric fluctuations during the night, we calibrate the observations of a science source frequently. We choose calibration sources that are unresolved (visibility amplitude greater than about 95%) and that are placed within about 5° of the science source in the sky. The normal mode of observing is to alternate observations between the science source and the calibrator in a time interval of order 5 minutes to minimize the effects of the atmosphere-instrument variations. Calibrated visibilities are obtained by dividing the observed visibility amplitude of the science source by the observed visibility amplitude of the calibrator, after correction for the estimated calibrator size. As we reported in Paper I, we have assigned an error of ± 0.051 to the calibrated visibility measured on a single night, based upon our experience with the scatter in the observed visibility for the same star over different nights; the error is decreased as the square root of the number of nights on which observations were made. This error and the visibility were used to compute the error in the UD diameter.

The referee has pointed out to us that the application of such a naive error estimate to the visibility might not be expected. For example, assuming photon statistics as the principal source of noise, one would expect the error to grow with increasing visibility for a source of fixed brightness. We have applied the error to the full range of visibility measurements. Furthermore, because of correlations in the two data channels resulting from atmospheric effects, it may not be reasonable to assume that using two channels reduces the error by $2^{1/2}$. We may justify the application of this simple visibility error estimate by considering all the repeated data available from this paper and Paper I, where the maximum baseline variation is no more than 4% among the observations. A random distribution in the projected baseline of $\pm 2\%$ around a mean baseline of 37.5 m produces an rms variation in the observed visibility of ± 0.0085 about a mean visibility of 0.55 for a star of angular diameter 8 mas. For all the stars in our program with two or more observations, we have computed the mean and the absolute deviation for each observation. These absolute deviations are plotted in Figure 3, as a function of the measured visibility, where the entire sample has been used. We note that the

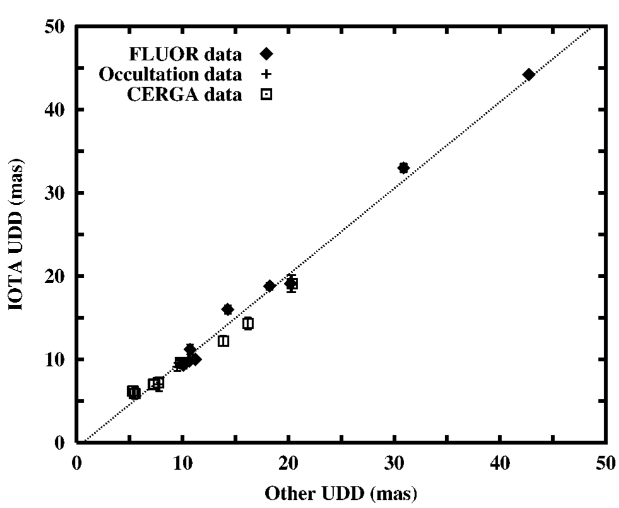

FIG. 2.—Comparison of UD angular diameter (UDD) observations made at IOTA with those obtained by other means. Sources for the other measurements are discussed in § 1. The line is the best fit to the data and is also discussed in the text.

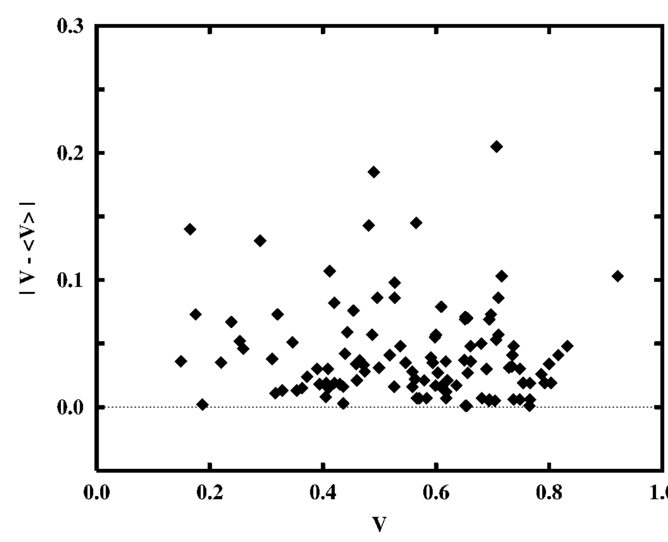

FIG. 3.—Plot of absolute visibility deviation vs. visibility for all stars measured in this paper and in Paper I that have observations on two or more nights. Note that there is no change of the scatter with observed visibility. See § 2 for a more detailed explanation.

TABLE 1

New Visibility and UD Diameter Data

Name	HR	Date	B_p (m)	V (mas)	θ_{UD} (mas)	Name	HR	Date	B_p (m)	V (mas)	θ_{UD} (mas)
β And	337	1995 Oct 5	36.71	0.196	12.2 ± 0.6	AT Dra	6086	1996 Jun 1	34.57	0.798	5.5 ± 0.7
γ^1 And	603	1995 Oct 5	37.06	0.644	7.0 ± 0.6	R UMi	…	1996 Jun 6	26.64	0.763	7.8 ± 0.9
α Ari	617	1995 Oct 8	38.24	0.722	5.9 ± 0.6	S Dra	…	1996 May 31	35.85	0.681	6.8 ± 0.6
RZ Ari	867	1995 Oct 8	38.25	0.430	9.1 ± 0.5			1996 Jun 1	34.80	0.694	6.9 ± 0.6
		1996 Oct 4	37.18	0.394	9.8 ± 0.6	V636 Her	6242	1996 May 30	37.54	0.758	5.6 ± 0.6
α Cet	911	1995 Oct 6	33.22	0.328	11.7 ± 0.6	IRC +40292	…	1996 May 29	36.83	0.832	4.7 ± 0.8
		1995 Oct 7	32.86	0.354	11.5 ± 0.6			1996 Jun 7	35.52	0.737	6.2 ± 0.7
BE Cam	1155	1996 Oct 6	33.07	0.630	8.1 ± 0.6	IRC −10359	…	1996 Jun 4	30.53	0.795	6.3 ± 0.8
ι Aur	1577	1995 Oct 8	38.23	0.694	6.3 ± 0.6	π Her	6418	1996 May 29	37.07	0.803	5.1 ± 0.7
119 Tau	1845	1995 Oct 8	38.26	0.429	9.1 ± 0.5			1996 Jun 7	35.51	0.766	5.8 ± 0.7
π Aur	2091	1995 Oct 5	36.63	0.517	8.5 ± 0.6	OP Her	6702	1996 May 28	37.23	0.729	6.0 ± 0.6
ρ UMa	3576	1996 Mar 9	32.22	0.758	6.5 ± 0.8	γ Dra	6705	1996 Jun 1	34.81	0.458	9.7 ± 0.6
RS Cnc	3639	1996 Mar 7	21.20	0.443	16.2 ± 1.0	98 Her	6765	1996 Mar 12	38.24	0.787	5.1 ± 0.7
α Lyn	3705	1996 Mar 12	38.24	0.606	7.2 ± 0.6	IQ Her	…	1996 Mar 12	38.21	0.765	5.4 ± 0.6
γ^1 Leo	4057	1996 Mar 10	36.80	0.563	8.0 ± 0.6			1996 Jun 2	37.22	0.800	5.1 ± 0.7
		1996 Mar 11	36.82	0.537	8.3 ± 0.6			1996 Jun 6	35.39	0.734	6.3 ± 0.7
		1996 Mar 12	38.13	0.655	6.7 ± 0.6	TU Lyr	…	1996 Jun 7	35.28	0.666	7.1 ± 0.6
72 Leo	4362	1996 Mar 12	38.21	0.742	5.7 ± 0.6	IRC −10414	…	1996 Jun 4	29.74	0.780	6.7 ± 0.8
λ Dra	4434	1996 Mar 9	31.23	0.721	7.3 ± 0.7	XY Lyr	7009	1996 May 29	37.37	0.527	8.3 ± 0.6
IRC +40226	…	1996 Mar 6	21.16	0.720	10.8 ± 1.1	δ^2 Lyr	7139	1995 Oct 8	38.25	0.411	9.3 ± 0.5
		1996 Mar 12	38.24	0.506	8.3 ± 0.5			1996 May 29	37.39	0.310	10.6 ± 0.6
ω Vir	4483	1996 Mar 17	34.51	0.730	6.5 ± 0.7	T Sge	…	1996 Jun 2	37.40	0.651	6.9 ± 0.6
RU Crt	…	1996 Mar 17	32.80	0.673	7.6 ± 0.7			1996 Jun 3	37.19	0.599	7.5 ± 0.6
Z UMa	…	1996 Mar 9	32.82	0.704	7.2 ± 0.7			1996 Jun 7	35.26	0.496	9.1 ± 0.6
BK Vir	…	1996 Mar 17	33.21	0.375	11.2 ± 0.6	CH Cyg	…	1996 Oct 7	37.07	0.336	10.4 ± 0.6
TU CVn	4909	1996 May 29	37.43	0.656	6.8 ± 0.6	AF Cyg	…	1996 May 28	36.88	0.745	5.9 ± 0.6
δ Vir	4910	1996 Mar 17	34.13	0.468	9.8 ± 0.6	IRC +20439	…	1996 Jun 2	37.38	0.438	9.2 ± 0.5
40 Com	4949	1996 Mar 10	37.41	0.598	7.5 ± 0.6	γ Sge	7635	1996 Jun 3	37.51	0.728	6.0 ± 0.6
		1996 Mar 11	37.41	0.652	6.9 ± 0.6	VZ Sge	7645	1996 Jun 7	35.48	0.716	6.5 ± 0.7
		1996 Mar 12	38.22	0.647	6.8 ± 0.6	AC Cyg	…	1996 May 31	34.61	0.735	6.4 ± 0.7
		1996 Jun 2	37.51	0.710	6.2 ± 0.6			1996 May 31	34.94	0.816	5.2 ± 0.8
BY Boo	5299	1996 May 30	37.32	0.636	7.1 ± 0.6	BC Cyg	…	1996 May 29	37.33	0.657	6.8 ± 0.6
		1996 Jun 6	35.50	0.658	7.2 ± 0.6	RS Del	…	1996 Jun 3	37.34	0.784	5.3 ± 0.6
CI Boo	…	1996 Jun 7	35.38	0.770	5.8 ± 0.7	RT Del	…	1996 Jun 2	37.41	0.736	5.9 ± 0.6
RV Boo	…	1996 Mar 6	21.20	0.737	10.4 ± 1.1	DY Vul	…	1996 Jun 7	35.34	0.681	6.9 ± 0.6
		1996 Mar 8	21.20	0.748	10.1 ± 1.1	RS Cap	…	1996 Jun 4	29.33	0.765	7.0 ± 0.8
HD 130144	5512	1996 Mar 11	37.02	0.518	8.4 ± 0.6	IRC +60305	…	1996 Oct 6	33.60	0.783	6.9 ± 0.7
		1996 Mar 12	38.13	0.486	8.5 ± 0.5	IRC +50383	…	1996 Jun 1	34.72	0.750	6.2 ± 0.7
β UMi	5563	1996 Jun 6	27.69	0.627	9.7 ± 0.8	RU Cyg	…	1995 Oct 4	35.06	0.526	8.8 ± 0.6
RR UMi	5589	1996 Jun 6	28.99	0.600	9.6 ± 0.7			1995 Oct 5	35.84	0.558	8.3 ± 0.6
FL Ser	5654	1996 Jun 2	36.98	0.593	7.6 ± 0.6	RV Cyg	…	1995 Oct 8	38.24	0.577	7.6 ± 0.5
IRC 00265	…	1996 Mar 17	34.52	0.667	7.3 ± 0.6	ε Peg	8308	1995 Oct 6	34.30	0.612	8.0 ± 0.6
		1996 Jun 4	31.59	0.773	6.4 ± 0.8			1996 Jun 3	37.30	0.565	7.9 ± 0.6
κ Ser	5879	1996 Mar 11	36.69	0.748	5.9 ± 0.7	GY Cyg	…	1996 May 31	35.26	0.754	6.0 ± 0.7
		1996 Jun 2	37.30	0.689	6.5 ± 0.6			1996 Jun 1	35.23	0.792	5.5 ± 0.7
ST Her	…	1996 May 29	36.75	0.420	9.6 ± 0.6	ζ Cep	8465	1996 Oct 6	34.05	0.800	5.6 ± 0.8
		1996 May 30	36.98	0.460	9.1 ± 0.6	SV Cas	…	1996 Oct 7	36.28	0.660	7.0 ± 0.6
		1996 Jun 1	35.64	0.451	9.5 ± 0.6	RS And	…	1996 Oct 7	36.33	0.629	7.4 ± 0.6
X Her	…	1996 Jun 1	35.82	0.149	13.1 ± 0.7	ψ Peg	9064	1996 Oct 4	37.65	0.694	6.4 ± 0.6
LQ Her	6039	1996 Mar 12	38.22	0.704	6.1 ± 0.6	30 Psc	9089	1995 Oct 6	33.18	0.694	7.2 ± 0.7
δ Oph	6056	1996 Mar 17	34.13	0.505	9.3 ± 0.6			1995 Oct 7	32.93	0.704	7.1 ± 0.7

upper limit to the deviations is about 0.2, with the bulk of the points lying at levels less than 0.1. In fact, four stars produce the points that deviate most widely from the rest of the sample. Notable among these is RX Boo, for which we reported the largest sample of repeated observations (see Paper I). This was done because we suspected at the time that RX Boo might show some time variability in the measured visibility. If we exclude RX Boo from the sample on the grounds that it may be variable, the rms fluctuation in the remaining stars in the distribution shown is ± 0.0526. Subtracting in quadrature the rms variation noted above for the dispersion caused by projected baseline changes from the observed visibility scatter in the sample yields a corrected estimate for the error of ± 0.0519. This is very close to the estimate obtained in Paper I made with a smaller data set and indicates that two detector channels are indeed better than one by about the expected factor; we adopt the error from Paper I for consistency. Note also that there is no correlation between the absolute deviation and the observed visibility over the approximate range $0.1 \leq V \leq 0.9$. In particular, there is no growth of error with increasing visibility, so we feel justified in applying a simple error estimate over the entire range of our visibility measurements. The observed distribution indicates only that sources of error other than photon statistics are important to the observations in the near-infrared.

In Table 2, we have converted the UD diameters to Rosseland mean diameters, using the relationship $\theta_R = 1.022\theta_{UD}$, adopted from Scholz & Takeda (1987; see Paper I for a discussion). Effective temperatures were computed

TABLE 2

DERIVED DATA

Name	HR	HD	Spectral Type	T_{eff} (K)	Reference	F_{bol} (W cm^{-2} μm^{-1})	θ_{UD} (mas)
β And	337	6860	M0+IIIa	4002 ± 178	1	1.33×10^{-12}	12.2 ± 0.6
γ^1 And	603	12533	K3−IIb	4470 ± 251	1	6.81×10^{-13}	7.0 ± 0.6
α Ari	617	12929	K2−IIIab	4790 ± 298	1	6.38×10^{-13}	5.9 ± 0.6
RZ Ari	867	18191	M6−III	3442 ± 148	1	4.32×10^{-13}	9.4 ± 0.4
α Cet	911	18884	M1.5 IIIa	3869 ± 161	1	1.05×10^{-12}	11.6 ± 0.4
BE Cam	1155	23475	M2+IIab	3550 ± 185	1	3.63×10^{-13}	8.1 ± 0.6
ι Aur	1577	31398	K3 II	4389 ± 263	2	5.13×10^{-13}	6.3 ± 0.6
119 Tau	1845	36389	M2 Iab–Ib	3823 ± 176	1	6.16×10^{-13}	9.1 ± 0.5
α Ori	2061	39801	M1–M2 Ia–Ib	3605 ± 43	1	1.15×10^{-11}	44.2 ± 0.2
π Aur	2091	40239	M3 II	3736 ± 190	1	4.90×10^{-13}	8.5 ± 0.6
ρ UMa	3576	76827	M3 IIIb	3279 ± 233	1	1.70×10^{-13}	6.5 ± 0.8
RS Cnc	3639	78712	M6 IIIase	3120 ± 126	3	8.47×10^{-13}	16.0 ± 0.5
α Lyn	3705	80493	K7 IIIab	3969 ± 220	1	4.48×10^{-13}	7.2 ± 0.6
γ^1 Leo	4057	89484	K1−IIIb	3949 ± 172	1	4.98×10^{-13}	7.7 ± 0.3
72 Leo	4362	97778	M3 IIb	3734 ± 238	1	2.20×10^{-13}	5.7 ± 0.6
λ Dra	4434	100029	M0 III	3526 ± 212	1	2.87×10^{-13}	7.3 ± 0.7
ω Vir	4483	101153	M4–M4.5 III	3544 ± 229	4	2.32×10^{-13}	6.5 ± 0.7
Z UMa	...	103681	M5 IIIvar	2596 ± 157	5	8.20×10^{-14}	7.2 ± 0.7
BK Vir	...	108849	M7−III:	3074 ± 141	1	3.90×10^{-13}	11.2 ± 0.6
TU CVn	4909	112264	M5−III	3350 ± 159	1	2.21×10^{-13}	7.1 ± 0.4
δ Vir	4910	112300	M3+III	3783 ± 182	1	6.85×10^{-13}	9.8 ± 0.6
40 Com	4949	113866	M5 III	3433 ± 148	3	2.27×10^{-13}	6.8 ± 0.3
BY Boo	5299	123657	M4.5 III	3506 ± 147	1	2.55×10^{-13}	7.0 ± 0.3
α Boo	5340	124897	K1.5 III	4628 ± 210	1	5.83×10^{-12}	19.1 ± 1.0
CI Boo	...	126009	M3 II	3227 ± 226	3	1.27×10^{-13}	5.8 ± 0.7
RX Boo	...	126327	M7.5–M8	2915 ± 113	1	8.85×10^{-13}	18.8 ± 0.4
IRC +20275	5512	130144	M5 IIIab	3577 ± 147	3	3.82×10^{-13}	8.2 ± 0.3
β UMi	5563	131873	K4−III	4086 ± 225	1	9.13×10^{-13}	9.7 ± 0.8
RR UMi	5589	132813	M4.5 III	3464 ± 179	1	4.62×10^{-13}	9.6 ± 0.7
FL Ser	5654	134943	M4 IIIab	2830 ± 152	3	1.29×10^{-13}	7.6 ± 0.6
τ^4 Ser	...	139216	M5 IIIa	3315 ± 135	1	4.20×10^{-13}	10.0 ± 0.3
κ Ser	5879	141477	M0.5 IIIab	3575 ± 185	1	2.22×10^{-13}	6.2 ± 0.5
ST Her	...	142143	M6–M7 III(S)	3319 ± 131	1	3.72×10^{-13}	9.4 ± 0.2
X Her	...	144205	M7	3281 ± 130	6	6.05×10^{-13}	12.2 ± 0.3
LQ Her	6039	145713	M4.5 IIIa	3457 ± 211	3	1.85×10^{-13}	6.1 ± 0.6
δ Oph	6056	146051	M0.5 III	3987 ± 168	1	7.58×10^{-13}	9.3 ± 0.4
AT Dra	6086	147232	M4 IIIa	3740 ± 272	3	2.06×10^{-13}	5.5 ± 0.7
g Her	6146	148783	M6−III	3449 ± 141	1	1.08×10^{-12}	14.8 ± 0.5
V636 Her	6242	151732	M4.5 III	3182 ± 205	1	1.12×10^{-13}	5.6 ± 0.6
α^1 Her	6406	156014	M5 Ib–II	3271 ± 46	1	4.34×10^{-12}	33.0 ± 0.5
π Her	6418	156283	K3 II	4106 ± 239	1	2.94×10^{-13}	5.4 ± 0.5
OP Her	6702	163990	M5 IIb–IIIa	3497 ± 175	4	1.64×10^{-13}	5.6 ± 0.4
γ Dra	6705	164058	K5 III	4095 ± 163	1	9.06×10^{-13}	9.6 ± 0.3
98 Her	6765	165625	M3−S III	3755 ± 289	1	1.80×10^{-13}	5.1 ± 0.7
IQ Her	...	168198	M4 II–M6 III	3502 ± 176	3	1.63×10^{-13}	5.6 ± 0.4
XY Lyr	7009	172380	M4.5–M5+II	3351 ± 143	1	2.26×10^{-13}	7.2 ± 0.3
δ^2 Lyr	7139	175588	M4 II	3637 ± 145	1	5.79×10^{-13}	9.7 ± 0.3
R Lyr	7157	175865	M5 III	3749 ± 164	3	1.23×10^{-12}	13.4 ± 0.6
CH Cyg	...	182917	M7 IIIvar	3084 ± 130	7	3.15×10^{-13}	10.0 ± 0.4
γ Aql	7525	186791	K3 II	4106 ± 174	1	5.53×10^{-13}	7.5 ± 0.3
δ Sge	7536	187076	M2 II	3779 ± 164	3	4.32×10^{-13}	7.8 ± 0.3
γ Sge	7635	189319	M0−III	4189 ± 238	1	3.24×10^{-13}	5.5 ± 0.5
VZ Sge	7645	189577	M4 IIIa	3844 ± 251	3	2.30×10^{-13}	5.5 ± 0.6
31 Cyg	7735	192577	K4 Ib	3466 ± 216	8	1.75×10^{-13}	5.9 ± 0.6
32 Cyg	7751	192909	K5 Iab	3543 ± 214	8	2.11×10^{-13}	6.2 ± 0.6
BC Cyg	...	...	M4 Ia	3673 ± 210	9	2.93×10^{-13}	6.8 ± 0.6
EU Del	7886	196610	M6 III	3508 ± 145	1	5.03×10^{-13}	9.8 ± 0.3
U Del	7941	197812	M5 II–III	3389 ± 155	3	2.83×10^{-13}	7.8 ± 0.4
EN Aqr	7951	198026	M3 III	3933 ± 286	1	2.52×10^{-13}	5.5 ± 0.7
ξ Cyg	8079	200905	K4.5 Ib–II	3491 ± 189	1	2.91×10^{-13}	7.5 ± 0.6
RS Cap	...	200994	M6–M7 III	3469 ± 234	10	2.47×10^{-13}	7.0 ± 0.8
IRC +60305	...	202380	M2 Ib	3774 ± 261	1	2.46×10^{-13}	5.9 ± 0.7
V1070 Cyg	...	203712	M7 III	3526 ± 164	11	3.07×10^{-13}	7.6 ± 0.4
W Cyg	8262	205730	M5 IIIae	3373 ± 143	3	5.88×10^{-13}	11.4 ± 0.5
ϵ Peg	8308	206778	K2 Ib–II	4459 ± 184	1	7.83×10^{-13}	7.5 ± 0.3
ζ Cep	8465	210745	K1.5 Ib	4246 ± 337	1	3.55×10^{-13}	5.6 ± 0.8
λ Aqr	8698	216386	M2.5 III	3477 ± 187	1	4.03×10^{-13}	8.9 ± 0.7
β Peg	8775	217906	M2.5 II–III	3890 ± 174	1	1.63×10^{-12}	14.3 ± 0.7
ψ Peg	9064	224427	M3 III	3475 ± 206	1	2.08×10^{-13}	6.4 ± 0.6
30 Psc	9089	224935	M3 III	3647 ± 184	1	3.15×10^{-13}	7.2 ± 0.5

REFERENCES.—(1) Keenan & McNeil 1989; (2) Morgan & Keenan 1973; (3) Hoffleit 1982; (4) Keenan 1963; (5) Keenan 1942; (6) Lockwood 1972; (7) Keenan & Hynek 1945; (8) Wright 1970; (9) Elias, Frogel, & Humphreys 1985; (10) Houk & Smith-Moore 1988; (11) Moore & Paddock 1950.

from these Rosseland mean diameters and bolometric fluxes estimated from broadband photometry. The photometric data were obtained from the SIMBAD database, where we have used the JP11 measurements when they were available. When photometric data were not available for some wavelengths, we filled in by interpolation using mean colors for the observed spectral type. The raw magnitudes were corrected for reddening, using the scheme described in Paper I, and integrated numerically to obtain the bolometric flux. Note that we have not computed effective temperatures for all stars reported in Table 1. Rather, we have restricted the sample to those stars that we judge to have well-determined spectral types; references to the sources for these spectral types are given in Table 2. We also included earlier observations from Paper I, bringing the total number of stars with effective temperature estimates to 70. Where there were overlapping data, we have averaged the UD diameters together, weighted by the error.

Random errors in the effective temperatures were computed by assuming an uncertainty of 15% in the bolometric flux (arising from errors in the absolute calibration, errors in the reddening estimate, and variability) and the computed error in the UD diameter listed in Table 2. The interested reader should consult Paper I for details of the error estimates for the bolometric flux.

3. DISCUSSION

3.1. *Effective Temperatures*

The effective temperatures for luminosity classes II, II–III, and III are plotted in Figure 4, where we have plotted only those stars for which the error in the temperature was ≤ 300 K. This resulted in 60 stars. We have also included the available occultation data from Ridgway et al. (1980), supplemented by a few additional stars reported in Paper I. The justification for combining the two data sets is based upon the analysis carried out in Paper I. In that paper (see its Table 5), we compared the effective temperature scale defined by Ridgway et al. (1980) with the one derived from IOTA interferometry. The result was that the IOTA scale was about 100 K cooler than the occultation scale at spectral type K1 III, but about 130 K warmer at spectral type M6 III. The intrinsic scatter at each spectral type was estimated to be about 100 K, so it seems reasonable to conclude that the two scales are identical. We have not replotted the stars observed at CERGA, since they overlap almost completely with the IOTA observations. The total number of effective temperatures determined from occultation measurements is 31, bringing the total number plotted in Figure 4 to 91 stars. This is nearly 50% more stars than were reported in Paper I.

One may note three general features in the figure. First, there is a uniform mix of IOTA interferometric and occultation temperatures. Each data set appears to cover the band defined by the other with no systematic separation. This is consistent with the conclusions given in Paper I. Second, all but eight of the stars are concentrated at the upper part of the distribution. The eight discordant stars form a parallel sequence offset by about 750 K to cooler temperatures from the average of the remaining 83 stars. Finally, at the scale shown in the figure, there is a linear decrease of temperature over the range of spectral types from G8 to M8.

Because we have mixed together luminosity classes II and III, it is of interest to determine whether the eight discordant stars in Figure 4 have luminosities systematically higher than the remainder of the stars. One might anticipate this effect based upon our previous result (Paper I) showing that supergiants have systematically lower temperatures than their giant counterparts at the same spectral type. The eight stars under discussion here are υ Leo, γ^1 Leo, 75 Tau, 6 Leo, 46 Leo, HD 75176, FL Ser, and Z UMa, all classified as luminosity class III. Two of the eight are known to be members of double systems, which could produce the observed effect, but the other stars appear to be single.

If we assume that the roughly linear relationship between spectral type and effective temperature shown in the figure is, in fact, correct, then we may determine an equation that will describe the temperature over this range of spectral types. A linear regression to all data except the eight discordant stars results in

$$T = 106\mathrm{ST} + 4580 \text{ K} ,$$

where the index ST has possible values $-2, \ldots, 0, \ldots, 5, 6, \ldots$, and 8, corresponding to spectral classes G8, ..., K0, ..., K5, M0, ..., and M8, respectively. The regression for the 83 stars yields a standard error for a single estimate of temperature of ± 192 K. If some other functional form better expresses the relationship between the spectral type and the effective temperature for giants, then this error is an upper limit to the average dispersion at each spectral class. We show this regression in Figure 4 for comparison with the observed data.

The error in the computed effective temperatures is divided between the uncertainty assumed for the bolometric flux density and the error in the measured angular diameter, with the error in the diameter yielding the greater contribution. The mean relative error in the angular diameter for the stars listed in Table 1 is $\sigma_\theta/\theta \approx \pm 0.09$, leading to an error contribution of $\pm 4.5\%$. For a star of effective temperature 3000 K, this corresponds to an error in the temperature of about ± 160 K. Taking a mean bolometric flux relative error of $\pm 15\%$, we obtain a contribution to the effective temperature error of $\pm 3.75\%$, or approximately ± 115 K for the star just mentioned.

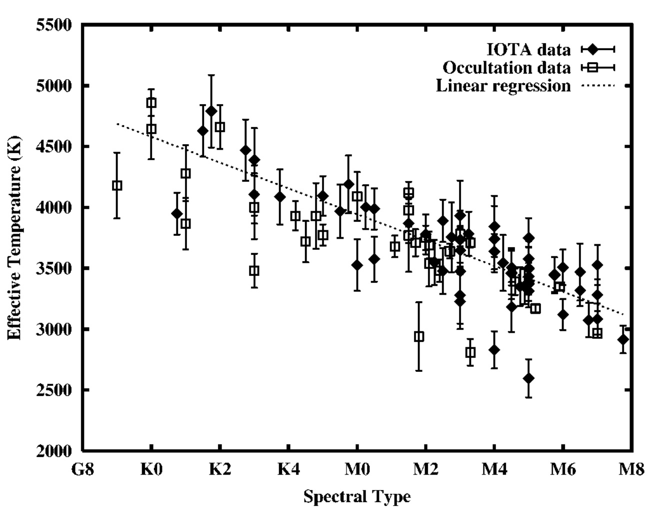

FIG. 4.—Plot of effective temperature vs. spectral type for luminosity class II, II–III, and III stars, comparing the results of lunar occultation observations with those from interferometry, all made at near-infrared wavelengths. The dotted line is a linear regression (see § 3.1).

3.2. *Stellar Radii*

We have searched the *Hipparcos* database with SIMBAD to find stars in our observed sample that have had accurate parallax determinations. Fewer than six of the stars listed in Table 2 have parallaxes that are less than 3 σ above the measurement errors. We have isolated stars classified as luminosity class II or II–III from those classified as luminosity class III. Data from these two groups are plotted in Figure 5 as stellar radius (in solar units) versus effective temperature, where class II and II–III stars are shown as squares and class III stars are shown as diamonds. One may see that there is a clear separation between the two luminosity classes, with the class II and II–III stars being larger than the class III stars. Around an effective temperature of 3500 K, the higher luminosity stars have approximately a factor of 2 larger radius, on average, than do the lower luminosity stars.

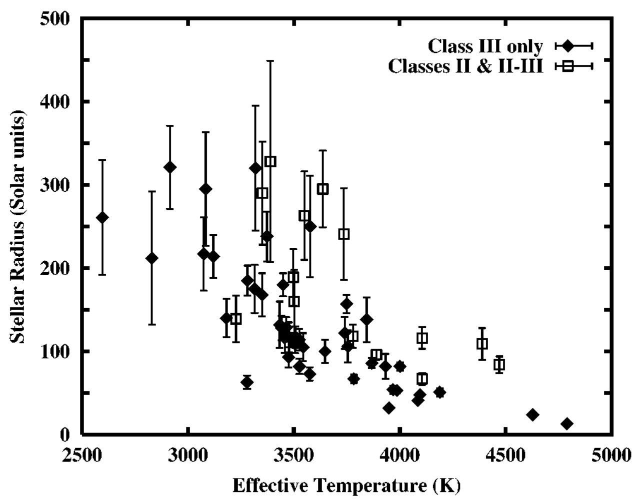

FIG. 5.—Plot of stellar radius as a function of effective temperature. Note that luminosity class II and II–III stars are systematically larger than luminosity class III stars at a given effective temperature.

The principal source of error in Figure 5 is still the error in the parallax. With increased precision in these measurements, it should be possible to establish quantitative values of radius corresponding to subtle spectroscopic luminosity differences. In fact, it is this limitation in establishing the distance to our sample of stars that prevents us from constructing an H-R diagram with the data at hand. While the parallaxes are often 5–10 σ results, a level of precision that allows us to see gross radius differences readily, the effect of computing luminosity is to increase the relative error by a factor of 2 (since distance enters as the second power). This yields an H-R diagram that is not even qualitatively useful.

This research has made use of the SIMBAD database, operated at CDS, Strasbourg, France. H. M. D. acknowledges support from NSF grant AST 95-8129 while he was at the University of Wyoming. G. T. v. B. was supported while he was a student at the University of Wyoming by a grant from the PASS Center. R. R. T. was similarly supported. Portions of this work were performed at the Jet Propulsion Laboratory, California Institute of Technology, under contract with NASA.

REFERENCES

Carleton, N. P., et al. 1994, Proc. SPIE, 2200, 152
Di Benedetto, G. P., & Ferluga, S. 1990, A&A, 236, 449
Di Benedetto, G. P., & Rabbia, Y. 1987, A&A, 188, 114
Dyck, H. M., Benson, J. A., & Ridgway, S. T. 1993, PASP, 105, 610
Dyck, H. M., Benson, J. A., van Belle, G. T., & Ridgway, S. T. 1996, AJ, 111, 1705 (Paper I)
Elias, J. H., Frogel, J. A., & Humphreys, R. M. 1985, ApJS, 57, 91
Hoffleit, D. 1982, The Bright Star Catalogue (4th rev. ed.; New Haven: Yale Univ. Obs.)
Houk, N., & Smith-Moore, M. 1988, Michigan Catalogue of Two-dimensional Spectral Types for the HD Stars, Vol. 4 (Ann Arbor: Univ. Michigan Dept. Astron.)
Keenan, P. C. 1942, ApJ, 95, 461
———. 1963, in Basic Astronomical Data, ed. K. A. Strand (Chicago: Univ. Chicago Press), chap. 8
Keenan, P. C., & Hynek, J. A. H. 1945, ApJ, 101, 265
Keenan, P. C., & McNeil, R. C. 1989, ApJS, 71, 245
Lockwood, G. W. 1972, ApJS, 24, 375
Moore, J. H., & Paddock, G. F. 1950, ApJ, 112, 48
Morgan, W. W., & Keenan, P. C. 1973, ARA&A, 11, 29
Perrin, G., Coudédu Foresto, G., Ridgway, S. T., Mariotti, J.-M., Traub, W. A., Carleton, N. P., & Lacasse, M. 1998, A&A, 331, 619
Ridgway, S. T., Joyce, R. R., White, N. M., & Wing, R. F. 1980, ApJ, 235, 126
Scholz, M., & Takeda, Y. 1987, A&A, 186, 200
Tuthill, P. G. 1994, Ph.D. thesis, Univ. Cambridge
White, N. M., & Feierman, B. H. 1987, AJ, 94, 751
Wright, K. O. 1970, Vistas Astron., 12, 147